Int J Clin Exp Med 2022;15(10):328-337
www.ijcem.com /ISSN:1940-5901/IJCEM0136778

Original Article

Multi-parametric magnetic resonance imaging and CT characteristics and the pathologic basis of monostotic fibrous dysplasia

Na Zhao[1*], Hanbang Wang[2*], Fei Gao[1], Bin Shi[1], Dong Chen[1], Jiangning Dong[1]

[1]Department of Radiology, The First Affiliated Hospital of USTC, Division of Life Sciences and Medicine, University of Science and Technology of China, Anhui Provincial Cancer Hospital, Hefei 230031, Anhui Province, China; [2]Department of Orthopaedics, Fuyang Hospital Affiliated of Anhui Medical University, Fuyang 236000, Anhui, China. [*]Equal contributors and co-first authors.

Received June 26, 2021; Accepted July 13, 2022; Epub October 15, 2022; Published October 30, 2022

Abstract: Purpose: To improve the diagnostic accuracy of monostotic fibrous dysplasia (MFD) and identifying its pathological basis by comparing multi-parametric magnetic resonance imaging (mp-MRI) and CT findings.Materials and methods: In total, this study included 55 patients with MFD. Among the 42 cases with MRI, 29 cases underwent diffusion-weighted imaging (DWI) examination, 15 cases underwent contrast-enhanced MR imaging, and 43 cases underwent plain CT scanning. We compared the morphological characteristics between mp-MRI and basic CT features to combine the radiological features with pathological findings. Results: Fifty-five cases of MFD showed expansive bone destruction (43/55, 78.2%) and slightly hyperintensity or hyperintensity lesions (41/42, 97.6%) with low-signal sclerosing margin (29/42, 69.0%) that were found on T2-weighted imaging. DWI showed hyperintensity (27/29, 93.1%), and the average apparent diffusion coefficient (ADC) value was $1.38\pm0.42\times10^{-3}$ mm^2/s. The ground-glass component on T2-weighted imaging was slightly hyperintense or hyperintense (29/29, 100%), with mild or moderate enhancement in 2 cases each (2/15, 13.3%) and obvious enhancement in 11 cases (11/15, 73.4%). Secondary aneurysmal bone cysts were seen in 3 cases (3/55, 5.5%). CT imaging showed ground-glass density (41/43, 95.3%) and a high-density sclerosis ring at the margin (35/43, 81.4%). Showing pathological proof, the normal cancellous bone was replaced with abnormal fibrous tissue. Conclusions: MFD has characteristic mp-MRI findings, such as hyperintensity on T2-weighted imaging inside lesions with a low signal sclerosing margin, hyperintensity on DWI, higher ADC value, and obvious enhancement. MRI can provide more information about pathological features and imaging findings of MFD than radiography and CT, and is an important diagonostic supplementation to use radiography and CT.

Keywords: Monostotic fibrous dysplasia, multi-parametric MRI, diffusion-weighted imaging, apparent diffusion coefficient, computed tomography

Introduction

Fibrous dysplasia of bone (FDB) is classified as a “benign bone tumor of undetermined nature” according to the classification of bone and soft tissue tumors in the 5th edition of 2020 and is no longer considered to be a bone tumor-like lesion [1]. The pathological feature of FDB is that the normal bone tissue is replaced by a large amount of fibro-osseous tissue. FDB accounted for 2.5% of bone tumors and 7% of benign bone tumors [2].

Although FDB represents a benign bone tumor, malignant transformation occurs in approximately 0.5%-4% of cases, most commonly in the polyostotic form [3]. It is the most common cause of skeletal dysplasia in adolescents [4], with 75% of the patients younger than 30 years of age [5].

Most FDB is found incidentally, based on mass, deformity, pathological fracture, and pain. FDB can be divided into two forms: the monostotic fibrous dysplasia (MFD) form and the polyostotic fibrous dysplasia (PFD) form, affecting a single bone and multiple bones [6]. The monostotic form is more common than the polyostotic form. In the monostotic form, it usually occurs in the long bones of the lower extremi-

ties, ribs, and skull. In the polyostotic form, it usually occurs in the femur, pelvis, and tibia [1]. The literature reports that lesions rarely occur in the vertebrae and metacarpal [7, 8].

Diffusion-weighted imaging (DWI) and intravoxel incoherent motion diffusion-weighted imaging (IVIM-DWI) have great value in evaluating the characteristics of tumor cell proliferation. The ADC value in the lesions is related to the cell density, which may narrow the range of differential diagnoses of uncertain lesions. To date, only a few studies have specifically assessed multi-parametric MRI (mp-MRI) characteristics, particularly DWI and contrast-enhanced characteristics, and their pathologic basis in FDB. In previous literature, most of the MFD was largely isointense with skeletal muscle on T1-weighted images. On T2-weighted images, lesions are typically heterogeneously hyperintense. MRI contrast enhancement was seen in all the contrast cases, FD may have patchy central enhancement, rim enhancement, homogeneous enhancement or any combination of these presentations. On both T1- and T2-weighted images, an outer hypointense rim is typically seen, and it corresponds with the sclerotic rim seen on radiographs. Previous literature only evaluated MFD from T1 and T2 signals and its enhancement features, and did not point out the obvious enhancement features, nor did they introduce the signals features of DWI and ADC images, and their pathologic basis, DWI and ADC signal characteristics are not mentioned [9].

It is not difficult to diagnose PFD by plain radiography and CT because of its expansive ground-glass appearance [10] and expansive and bone destruction, bone deformation. However, the MFD on plain radiography often presents as a single osteolytic lesion. Especially when the swelling of the lesion was not obvious, the composition of ground glass is less ovbious, the sclerosing margin is incomplete, and secondary aneurysmal bone cyst or secondary pathological fracture with hemorrhage, plain radiography are often difficult to diagnose, and is not easy to differentiate from other fibrogenic tumors of bone, giant cell tumors of bone, single plasmacytoma, and Langerhans cell histiocytosis. The advantage of MRI is that MRI can more clearly show the pathological components and bleeding components of the lesions. The enhanced features of MRI are more obvious than those of CT, and DWI and ADC images features assist in the diagnosis.

The purpose of this study is to analyze detailed characteristics of DWI and contrast-enhanced MR images, combined with conventional imaging signs and CT-assisted findings, and then compared them with the pathological findings, to improve the understanding of the detailed image features of MFD.

Materials and methods

Patients and clinical information

The patient's information was retrieved from the Hospital Information System (HIS) at our hospital, between July 2012 and July 2020, there were 55 patients with pathologically confirmed MFD. This retrospective cohort study was approved by the institutional review committee. Due to the retrospective nature of the study, the requirement of informed consent was abandoned for this article, the institutional review board was the review board of Anhui Provincial Cancer Hospital (the West Branch of the First Affiliated Hospital of USTC, University of Science and Technology of China).

The clinical and imaging data of 55 patients with MFD confirmed by pathology after surgery (39 cases) and biopsy (16 cases) was from 29 males and 26 females. The patient's ages ranged from 7 to 63 years; the average age was 32.9±15.4 years old. The clinical data for the disease are shown in **Table 1**.

Inclusion criteria were as follows: (1) All cases were found for the first time, and MFD was confirmed by postoperative pathology; (2) the disease consisted of a single lesion in a single bone; and (3) preoperative examination, surgery, and pathology were completed in our hospital. Exclusion criteria were as follows: (1) The pathological diagnosis of MFD was doubtful, or the lesion was complicated with other bone diseases; (2) the disease was recurrent; and (3) multiple lesions appeared in a single bone or multiple bones.

MRI examination: MRI was performed using a 3.0-T system (GE Signa HDxT, GE Healthcare) that was equipped with an 8-channel phased-array coil. MR acquisitions, including axial fast

Table 1. Clinical data of 55 cases of MFD

Variable		No. of cases
Gender	Female	26
	Male	29
Age	≤20	15
	20-40	18
	≥40	22
Pathology confirmed	Confirmed by surgical pathology	39
	Confirmed by biopsy	16
Examination	Only CT examination performed	43
	Only MR examination performed	42
	CT and MR examinations were performed simultaneously	30
	Diffusion-weighted imaging (DWI)	29
	MR enhancement	15
Tumor site	Femur	16
	Tibia	14
	Ilium	6
	Sacrum	4
	Skull	4
	Ribs	3
	Humerus	3
	Lumbar spine	2
	Metatarsal	1
	Fibula	1
	Radius	1
Secondary aneurysmal bone cyst	Yes	3
	No	54
Pathological fracture	Yes	4
	No	51
Clinical symptoms	Pain or discomfort	37
	No symptoms, physical examination, or other examination findings	18

MFD: monostotic fibrous dysplasia, DWI: diffusion-weighted imaging.

spin-echo (FSE) T1-weighted (T1W) images, axial FSE T2W images, fat-suppressed T2-weighted (FS T2W) images, and axial diffusion-weighted imaging (DWI). T1W imaging parameters are as follows: repetition time/echo time (TR/TE) 500/7.8 ms, thickness 4.0 mm, number of excitations (NEX) 1. T2W imaging protocols are as follows: TR/TE 4200/68 ms, thickness 4.0 mm, and NEX 2. FS T2W imaging protocols are as follows: TR/TE 4200/68 ms, thickness 4.0 mm, and NEX 2. DWI: TR/TE 4000/65 ms, thickness 4.0 mm, and NEX 6, and b value 0 or 1000 s/mm^2. A power injector was used to inject the contrast material 0.1 mmol/kg, gadodiamide (Omniscan, GE Healthcare). The elbow vein was used for bolus injection and then scanned with T1W at a flow rate of 4 ml/s. After the contrast agent was injected, it was washed with 20 ml saline. The parameters of the LAVA-flex sequence are as follows: TR/TE 4.5/1.3 ms, flip angle 15, NEX 1, and bandwidth 166.67 kHz. One case was underwent Axial IVIM-DWI, with FS obtained in the short time inversion recovery (STIR) sequence using single-shot echo-planar imaging (EPI) pulse sequence with 10 b values (0, 10, 20, 50, 100, 200, 400, 800, 1,200 and 1,500 s/mm^2), TR/TE: 4,000/65 msec, NEX: 6).

CT examination: Forty-three of the 55 cases were examined using a GE Discovery CT750 HD CT scanner (GE Healthcare, Waukesha, WI).

The tube voltage was 120 kV, the tube current was 200 mA, the scanning field was 20-40 cm, the matrix was 512×512, and the thickness was 1.25 mm with a soft tissue algorithm in reconstruction and multiple planar reformations with 1.25 mm thickness to coronal planar reformation.

Radiologic evaluation

The consensus evaluation of the imaging features was reviewed on an Advantage Windows workstation 4.6 (AW 4.6 workstation, GE Healthcare) by two radiologists with 10 and 18 years of experience in musculoskeletal imaging. If lesions in two or more bones were found, the FDB was rated as polyostotic and otherwise as monostotic. The following CT and MRI features were recorded: size (maximum length; cm); present or not (ground glass, expansive bone destruction, marginal sclerosis, aneurysmal bone cyst (ABC)); invasion site; the signal intensity of lesions on T2W images, FS T2W images, and DWI (hypo-, iso-, and hyperintensity, compared with the adjacent bone); and ADC values (the software Function Tool was used to measure the ADC value of the tumors). Based on DWI and ADC images, the signal characteristics of bone lesions on two images were analyzed, and the ADC values of lesions were measured. The ROI area was kept consistent, avoiding hemorrhage, necrosis, blood vessels, and other components whenever possible; each ROI was measured three times to calculate the mean ADC value (mm^2/s).

Histopathology evaluation

Surgical or biopsy specimens were fixed with a formaldehyde solution, embedded in paraffin, stained with hematoxylin and eosin (H&E), and observed under light microscopy.

Results

Clinical data and histopathology findings

The 55 patients with MFD were confirmed by pathology; among them, 39 cases were confirmed by surgical pathology, and 16 cases were confirmed by biopsy. CT examination was performed in 43 cases, MR examination in 42 cases, both CT and MR examinations for 30 cases, and MR enhancement in 15 cases. The presenting complaint was pain or discomfort in 37 (66.3%) and physical examination or other examination findings in 18 (32.7%) of the cases. Clinically, pathological bone fractures were encountered in 4 (7.3%) cases. The length of the lesions was between 2.1 cm-16.4 cm. The lesions occurred in 6 cases of the iliac bone, 4 cases of sacrum and skull, 3 cases of rib, 2 cases of the lumbar spine, and 1 case of metatarsal bone; the rest were located in the long bones of limbs (**Table 1**).

Features of MRI and supplemental CT imaging and their correspondence with pathological findings

MR imaging manifestations: The lesions were iso-intense or hypointense on T1W images, with small spots of lower signal and slight hyperintensity or hyperintensity on T2W imaging in 97.6% (41/42). Pathologically, the lesions were mainly composed of proliferative spindle-forming fibroblasts and immature woven bone. The interstitium contained abundant thin-walled blood vessels with a low signal sclerosis margin of 69.0% (29/42). DWI showed medium and high signal intensity in 93.1% (27/29); the average ADC value was approximately $1.38\pm 0.42\times10^{-3}$ mm^2/s, and; the ground-glass component on T2W images was slightly hyperintense or hyperintense in 100% (29/29). Fifteen cases from this group underwent enhanced MRI scanning (compared with skeletal muscles of the same layer, a degree of enhancement similar to that of skeletal muscles was considered a mild enhancement, and a degree of enhancement that was significantly higher than that of skeletal muscles was considered an obvious enhancement, and a degree of enhancement between mild and obvious was considered moderate enhancement). After contrast enhancement, mild and moderate were found in 2 cases each and markedly enhanced in 11 cases (**Figures 1**-**3** and **Table 3**). Secondary aneurysmal bone cysts were seen in 5.5% (3/55) (**Tables 1**, **2**).

CT and MRI revealed that the manifestation was intra-osseous expansive bone destruction in 78.2% of cases (43/55). CT was combined with different degrees of ground-glass density in 94.9% (41/43). CT showed a ground-glass appearance at the edge of lesions or the edge of the bony septum.

In one case of MFD, a 13 year old female girl who had right thigh pain, underwent a conven-

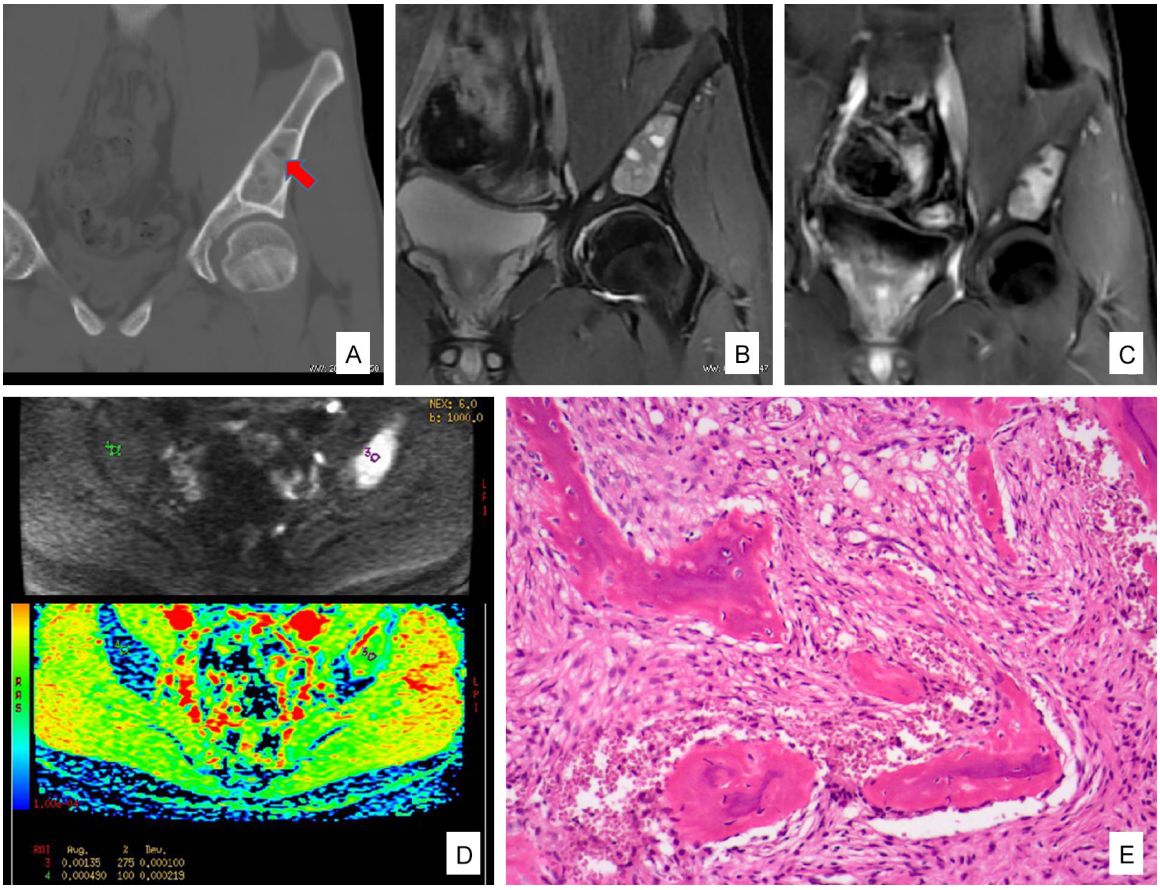

Figure 1. Male, 21 years old, fibrous dysplasia of the left iliac wing. (A) Shows a lesion in the left iliac bone with large ground glass density with some cystic changes in the center (red arrow). A sclerosing margin was seen around the lesion. (B) Shows a slightly high signal intensity in the ground-glass component on FS T2W imaging and higher signal intensity in the corresponding cystic degeneration region. (C) Shows obvious enhancement in the ground-glass areas. (D) Shows that DWI (b=1000 s/mm^2) was hyperintense in the lesion, with an ADC value of 1.35×10^{-3} mm^2/s and an ADC value of 0.49×10^{-3} mm^2/s in the contralateral normal bone. (E) Shows the immature woven bone under the microscope. Fibroblast proliferation was seen between trabeculae (H&E staining ×100).

tional MRI with IVIM-DWI. FS T2W imaging showed mixed signals in the lesion, mainly with inhomogeneous hyperintense lesion with small hypointense foci within it. Coronal contrast-enhanced fat-suppressed T1W showed most of the lesions were patchy enhancement. The T2 hyperintense area may represent the enhancing fibrous tissue. The IVIM-DWI images showed that the lesion IVIM-DWI (b=1200 s/mm^2) had a high signal, and the ADC value is 1.79×10^{-3} mm^2/s. The D (diffusion coefficient) value was 1.15×10^{-3} mm^2/s. The D* (pseudo diffusion coefficient) value was 3.22×10^{-3} mm^2/s, and The f (microvascular volume fraction) value was 66.6% (**Figure 2D**). The pathological findings showed there were no obvious osteoblasts around bone trabeculae, and fibrous tissue proliferation in the medullary cavity and multiple thin-walled vascular (yellow arrow) were also seen (**Figure 2E**).

Gross pathological manifestations included the following: bone swelling, bone cortex thinning, marrow cavity disappearance, and proliferated fibrous tissue replacement with gray or gray-red texture and a gritty feeling. There may have been cystic changes in the lesion, which may have been mucous, serous, or bloody fluid. Microscopically, lesions were mainly composed of proliferative spindle-forming fibroblasts and immature woven bone. Bone trabeculae were disordered, irregularly arranged, nonpolar, alphabetical, comma-like, fishhook-like, surrounded by no osteoblasts, and containing interstitial, rich, thin-walled blood vessels (**Figure 1E**).

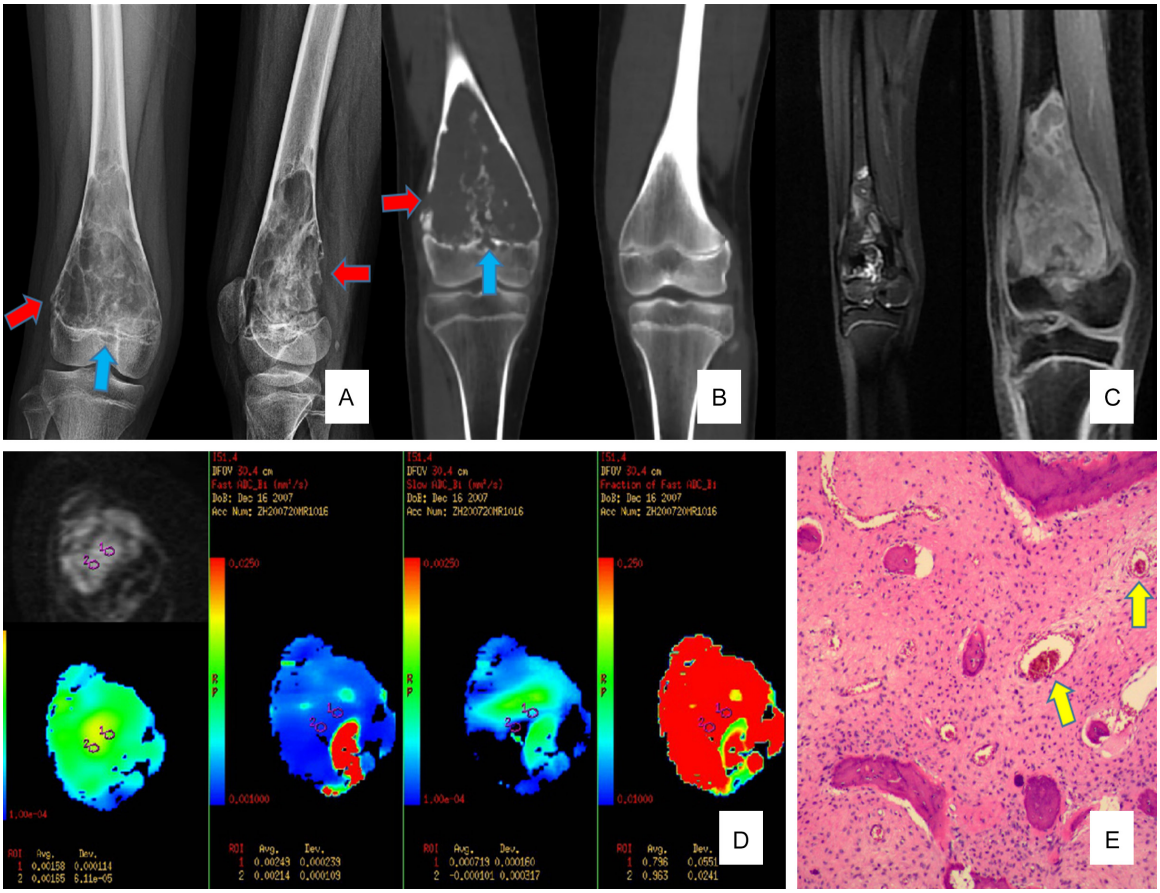

Figure 2. Female, 13 years old, fibrous dysplasia of the right femur. In (A), Radiography of the femur shows that there was a slight swelling irregular osteolytic bone destruction area in the medullary cavity of the right distal femur, which was multilocular, with matrix calcifications but no sclerotic rim, and it shows breaking through the bone cortex (red arrow) and the epiphyseal plate (blue arrow). (B), CT can more clearly show the destruction of bone cortex (red arrow) and breakthrough of epiphyseal plate (blue arrow), and shows multiple irregular ground glass ossification and calcification in the lesions. (C), FS T2W imaging shows mixed signals in the lesion, mainly with inhomogeneous hyperintense lesion with small hypointense foci within it showing patchy obvious enhancement of most of the lesion. (D) Shows that the lesion IVIM-DWI (b=1200 s/mm^2) has a high signal, and the ADC value is 1.79×10^{-3} mm^2/s. The D (diffusion coefficient) value was 1.15×10^{-3} mm^2/s. The D* (pseudo diffusion coefficient) value was 3.22×10^{-3} mm^2/s, The f (microvascular volume fraction) value was 66.6%, which showed that the blood supply of the lesion was very rich. (E) Shows there are no obvious osteoblasts around bone trabeculae, and fibrous tissue proliferation in the medullary cavity and multiple thin-walled vascular (yellow arrow) was also seen (H&E staining ×100).

Discussion

The pathophysiological mechanism of monostotic fibrous dysplasia

MFD is one form of FDB, with abnormal differentiation of osteoblasts leading to the replacement of normal cancellous bone by immature bone and fibrous stroma [11]. Bone trabeculae are derived from a fibrous matrix. The main characteristic under light microscopy is the lack of osteoblasts around the bone trabeculae surface.

FDB is a genetic bone disease with mutations in the guanine nucleotide-binding protein-1 (GNAS1) gene (chromosome 20q13.32) in osteoblastic lineage cells [12]. The mutation of GNAS1 impairs the function of Gsα-GTPase and inhibits the function of adenylate cyclase, which is the producer of cAMP, resulting in increased cyclic adenylate (cAMP) activity and abnormal differentiation of osteoblasts and leading to abnormal proliferation of intraosseous fibrous tissue and abnormal immature trabeculae. Constitutive activation increases bone resorption in FDB lesions [13].

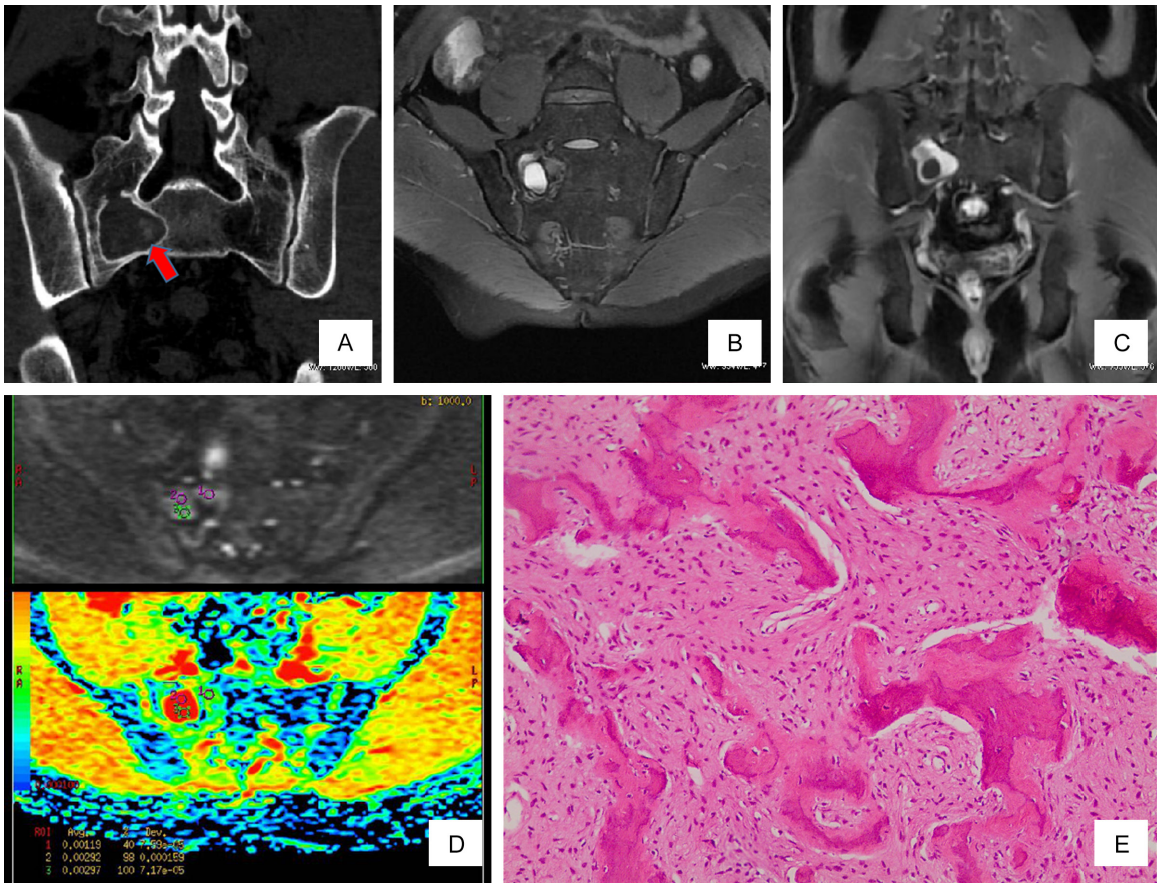

Figure 3. Male, 30 years old, fibrous dysplasia of the right sacrum. In (A), CT shows a circular low-density lesion on the right sacrum, with a few patchy ground-glass-like densities (red arrow) and an annular sclerosing margin around it. In (B), FS T2W imaging shows a slightly higher signal for the ground-glass composition. (C) Shows heterogeneous enhancement of the lesion and homogeneous enhancement of the ground glass areas. (D) Shows that the DWI of the ground-glass component (b=1000 s/mm^2) has a high signal, and the ADC value is 2.36×10^{-3} mm^2/s. (E) Shows fibrous tissue proliferation with irregular ossification under microscopy and no osteoblast proliferation around ossified trabeculae (H&E staining ×100).

Expansive destruction without soft tissue mass of the involved bone, with either thickening or thinning of the cortical bone, but penetrating destruction of the cortical bone is rare. This often occurs without cortical disruption or periosteal reaction, same as previous literature reports [14, 15], and a narrowing or disappearing bone marrow cavity, which is replaced by fibrous tissue with a gray or gray-red texture and a gritty feeling. There may be cystic changes in the lesions, with mucous, serous, or bloody fluid inside.

Microscopically, FDB is occurs the normal bone tissue is replaced by a large number of fibro-osseous tissue that contains irregular bony trabeculae of woven bone [12]. A large number of small vessels are found in the center of the lesions [16]. Bone trabeculae are disordered and irregularly arranged with no osteoblasts around them. The interstitium is rich in thin-walled vessels, myxoid degeneration, cystic degeneration, or secondary aneurysmal bone cysts can also be seen [17, 18].

Plain MRI scanning, DWI, and contrast enhancement features of monostotic fibrous dysplasia and its pathologic basis

The signal intensity of MFD on T1W and T2W images and the degree of contrast enhancement depend on the degree of fibrous tissue proliferation and the ratio of regenerate trabeculae, sclerosis, and calcification, and the amount and degree of cystic and hemorrhagic changes [9, 19]. The most common imaging

Table 2. MRI and CT imaging features of MFD in 55 cases

MFD imaging features	cases	%
Expansive bone destruction	43/55	78.2
High or slightly high signal on T2WI	41/42	97.6
High signal on T2WI in the lesion with ground-glass on CT	29/29	100
High signal on DWI	27/29	93.1
Low-signal sclerosing margin	29/41	70.7
CT combined with ground-glass composition	41/43	95.3
CT shows marginal sclerosis	35/43	81.4
Aneurysmal bone cyst (ABC)	3/55	5.5

MFD: monostotic fibrous dysplasia, DWI: diffusion-weighted imaging.

Table 3. MR enhancement characteristics of 15 cases of MFD

MRI enhancement degree	cases	%
Mild enhancement	2/15	13.3
Moderate enhancement	2/15	13.3
Significant enhancement	11/15	73.4

MFD: monostotic fibrous dysplasia.

feature of FDB is intraosseous expansive bone destruction with a homogeneous ground-glass appearance, which is described in approximately 97% of FDB cases [20]. When the lesions manifest as ground-glass density on CT, they are made of regenerate trabeculae and immature woven bone, which is the common characteristic manifestation of MFD. On CT, the lesions manifest with disappearing normal bone trabeculae and a blocked medullary cavity, leading to the ground-glass image performance. Most of these changes on MRI are slightly hyperintense or hyperintense on T2W images. This signal feature is mainly composed of proliferative spindle-forming fibroblasts, immature woven bone, and plenty of thin-walled blood vessels in the interstitium. The active metabolism and high water content of the lesion also result in the slightly hyperintense or hyperintense appearance on T2W images [21]. There were 3 cases combined with aneurysmal bone cysts, related to its abundant blood supply, and prone to myxoid degeneration, cystic degeneration, and a large number of blood sinuses [7]. The ratio of lesions containing low signal sclerotic margins was 29/42 (69.0%). It was hypointense on both T1W and FS T2W images, the same as previous literature reports [22], with a high-density sclerotic margin on CT. It is believed that the pathogenesis is the continuous ossification and calcification of fibrous tissue and bone trabeculae in the chronic expansive growth of the lesions, which reflects the characteristics of slow growth and benign bone tumors.

The 29 cases of MFD showed hyperintensity on DWI, with a mean ADC value of 1.38± 0.42×10^{-3} mm^2/s. The lesions were hypointense on DWI, but the ADC values were not low. There were almost no reports of DWI appearance and ADC value in the previous literature. This finding may be related to its abundant blood supply and T2W shine-through effect, which are characteristics of a benign tumor. Fibrous tissue in FDB lesions is highly vascularized [6]. In our study, approximately 13/15 (86.7%) of the 15 cases of MFD showed moderate to obvious enhancement at the venous phase (**Figures 1**-**3**). Mentioned in previous literature [23, 24], MRI contrast enhancement was seen in all the contrast cases, FD may have patchy central enhancement, rim enhancement, homogeneous enhancement, or any combination of these presentations. It is not mentioned that the lesion can be significantly enhanced, which is different from the literature. This was related to the metabolically active proliferating fibroblasts in the bone fibers, the abundant thin-walled small vessels among the fibroblasts, the immature woven bone stroma, and the abundant peripheral blood sinuses [24]. This finding also proves that the disease is a benign fibroid bone tumor, a type of blood-rich bone supply tumor, which explains why it easily merges with aneurysmal bone cysts. Histopathologically, ABC showed a spongy space filled with blood and occasionally endothelial cells [25]. These pathological findings were also consistent with those of thrombotic aneurysms [26, 27].

One case of MFD, a 13 year old female girl, illustrates that MRI is superior to radiography and CT in showing breaking through of the epiphyseal plate, involving epiphyseal signs with its complex components. The f (microvascular volume fraction) value was 66.6%, which showed rich blood supply characteristics in the lesions, and the pathology confirmed that the tumor had abundant blood vessels. The D

(diffusion coefficient) value indicated benign tumor characteristics, but it has invasive performance, which breaks through the epiphyseal plate and epiphyseal has been involved.

In the summary, the authors present the following findings. (1) Although MFD is composed of fibrous components and ground-glass ossification, the slightly hyperintense or hyperintense results of T2W or FS T2W images indicate that there are plenty of dilated blood vessels inside, which indirectly indicates a blood-rich tumor. (2) The hyperintensity of MFD on DWI may be related to the T2 shine-through effect. (3) Approximately 13/15 of the lesions showed moderate to obvious enhancement, indicating abundant thin-walled small vessels in the interstitium and a large number of blood sinuses around it, which further reflected a blood-rich bone tumor. (4) The low signal ring of margin on MRI is equivalent to the marginal sclerosing ring-jujube putamen sign on CT, which is related to the chronic expansive growth of tumors, and further reflects the characteristics of benign tumors.

Our study has several limitations. First of all, the sample size of this study was relatively small, especially for the enhanced cases (only 15 cases). Advanced statistical means should be added. Second, the enhancement time-intensity curves were not given in this study, because not all cases had dynamic contrast enhancement. Some cases had two phases of enhancement. Third, Pathological findings were not consistent with MRI and CT manifestations. Lastly, this study was a retrospective and there might be certain biases. This is a descriptive article of a retrospective experience summary. There are only simple percentage statistics. We will collect more cases for statistical analysis in the later stage.

In conclusion, FDB has characteristic MRI findings, which are well correlated with morphological and histopathological findings. They showed slightly hyperintense or hyperintense lesions with a low signal sclerosing margin on T2W or FS T2W images. Obvious enhancement, hyperintensity on DWI, and a high ADC value may be important radiologic signs of MFD. Most MFD can be observed as a single osteolytic and slight expansive bone destruction with varying degrees of ground-glass density on CT. MRI can provide more information about pathological features and imaging findings of MFD than plain radiography and CT, and is an important supplement to plain radiography and CT.

Acknowledgements

This study was supported by Key Specialties in Clinical Medicine Construction Funding Project of Anhui Province (No. 2019sjlczdzk).

Disclosure of conflict of interest

None.

Address correspondence to: Jiangning Dong, Department of Radiology, The First Affiliated Hospital of USTC, Division of Life Sciences and Medicine, University of Science and Technology of China, Anhui Provincial Cancer Hospital, No. 107, Huanhu East Road, Shushan District, Hefei City 230031, Anhui Province, China. E-mail: dongjn@163.com

References

[1] Siegal GP, Bloem JL, Cates JMM and Hameed M. Fibrous dysplasia. In: WHO classification of tumors •5th Edition of soft tissue and bone Tumours. Lyon: IARC Press, 2020: 472-474.

[2] Itshayek E, Spector S, Gomori M and Segal R. Fibrous dysplasia in combination with aneurysmal bone cyst of the occipital bone and the clivus: case report and review of the literature. Neurosurgery 2002; 51: 815-818.

[3] Rahbar R, Rodriguez-Galindo C, Meara JG, Smith ER and Perez-Atayde AR. Fibrous dysplasia. Pediatric head and neck tumors, 1st ed. New York: Springer; 2014. pp. 139-147.

[4] Kim YH, Song JJ, Choi HG, Lee JH, Oh SH, Chang SO, Koo JW and Kim CS. Role of surgical management in temporal bone fibrous dysplasia. Acta Otolaryngol 2009; 129: 1374-1379.

[5] Kransdorf MJ, Moser RP Jr and Gilkey FW. Fibrous dysplasia. Radiographics 1990; 10: 519-537.

[6] Hofmann E and Prescher A. The clivus anatomy, normal variants and imaging pathology. Clin Neuroradiol 2012; 22: 123-39.

[7] Ropper AE, Cahill KS, Hanna JW, McCarthy EF and Gokaslan ZL. Primary vertebral tumors: a review of epidemiologic, histological, and imaging findings, Part I: benign tumors. Neurosurgery 2011; 69: 1171-1180.

[8] Batista KT, Araujo HJ and Schwartzman UP. Monostotic fibrous dysplasia of the metacarpal: a case report. Rev Braz Ortop 2016; 51: 730-4.

[9] Damon K, Alexandra H, Ingo G, Kay Geert AH, Bernd H and Thomas E. Magnetic resonance

imaging features of craniofacial fibrous dysplasia. J Polish Journal Radiology 2019; 84: e16-e24.
[10] Lisle DA, Monsour PA and Maskiell CD. Imaging of craniofacial fibrous dysplasia. J Med Imaging Radiat Oncol 2008; 52: 325-332.
[11] Shah ZK, Peh WC, Koh WL and Shek TW. Magnetic resonance imaging appearances of fibrous dysplasia. Br J Radiol 2005; 78: 1104-15.
[12] Özşen M, Yalçinkaya Ü, Bilgen MS and Yazici Z. Fibrous dysplasia: clinicopathologic presentation of 36 cases. Turk Patoloji Derg 2018; 34: 234-241.
[13] Dicaprio MR and Enneking WF. Fibrous dysplasia. Pathophysiology, evaluation, and treatment. J Bone Joint Surg Am 2005; 87: 1848-1864.
[14] Sundaram M. Imaging of Paget's disease and fibrous dysplasia of bone. J Bone Miner Res 2006; 21 Suppl 2: P28-30.
[15] Saglik Y, Atalar H, Yildiz Y, Basarir K and Erekul S. Management of fibrous dysplasia. A report on 36 cases. Acta Orthop Belg 2007; 73: 96-101.
[16] Utz JA, Kransdorf MJ, Jelinek JS, Moser RP and Berrey BH. MR appearance of fibrous dysplasia. J Comput Assist Tomogr 1989; 13: 845-851.
[17] Kaloostian SW, Vartanian TK, Ordookhanian C, Vartanian T and Kaloostian PE. Concomitant fibrous dysplasia with aneurysmal bone cyst formation within the skull, humerus and rib. J Surg Case Rep 2018; 2018: rjy180.
[18] Nguyen BD, Lugo-Olivieri CH, McCarthy EF, Frassica FJ, Ma LD and Zerhouni EA. Fibrous dysplasia with secondary aneurysmal bone cyst. J Skeletal Radiology 1996; 25: 88-91.
[19] Kushchayeva YS, Kushchayev SV, Glushko TY, Tella SH, Teytelboym OM, Collins MT and Boyce AM. Fibrous dysplasia for radiologists: beyond ground glass bone matrix. Insights Imaging 2018; 9: 1035-1056.
[20] Savu AM, Manea C and Sarafoleanu C. Diagnostic difficulties in fibrous dysplasia a case series and a literature review. J Rom J Rhinol 2014; 4: 211-219.
[21] Chong VF, Khoo JB and Fan YF. Fibrous dysplasia involving the base of the skull. AJR Am J Roentgenol 2002; 178: 717-720.
[22] Shah ZK, Peh WC, Koh WL and Shek TW. Magnetic resonance imaging appearances of fibrous dysplasia. J Br J Radiol 2005; 78: 1104-1115.
[23] Gwark JY, Jeong JH, Hwang SC, Nam DC, Lee JH, Na JB and Kim DH. Monostotic fibrous dysplasia in the proximal tibial epiphysis: a case report. J Med Case Rep 2014; 8: 1-4.
[24] Butt A, Patel K, Agrawal K, Arya A and Singh J. Fibrous dysplasia of the clivus - a case study and literature review. Radiol Case Rep 2020; 16: 230-236.
[25] Gan YC and Hockley AD. Aneurysmal bone cysts of the cranium in children. Report of three cases and brief review of the literature. J Neurosurg 2007; 106 Suppl: 401-6.
[26] Yamashita S, Kimura H, Kohta M, Fujita A and Kohmura E. Thrombosed middle meningeal artery aneurysms mimicking aneurysmal bone cysts in a patient with fibrous dysplasia. World Neurosurg 2019; 130: 439-44.
[27] Rau LH, Reinheimer A, Meurer MI, Marodin AL, Espezim CS, Klüppel LE, Dos Santos Vaz Fernandes PC and Rivero ERC. Fibrous dysplasia with secondary aneurysmal bone cyst-a rare case report and literature review. Oral Maxillofac Surg 2019; 23: 101-107.